Available online at www.sciencedirect.com
SCIENCE DIRECT
Sensors and Actuators A 126 (2006) 122–128
SENSORS AND ACTUATORS A PHYSICAL
www.elsevier.com/locate/sna

Thermal and thermal stress analysis of a thin-film thermoelectric cooler under the influence of the Thomson effect

Mei-Jiau Huang [a,*], Po-Kuei Chou [a], Ming-Chyuan Lin [b]

[a] *Mechanical Engineering Department, National Taiwan University, Taiwan, ROC*
[b] *National Synchrotron Radiation Research Center, Taiwan, ROC*

Received 20 May 2005; received in revised form 7 September 2005; accepted 9 October 2005
Available online 28 November 2005

Abstract

This work has two parts. The first part details the thermal analysis of a thin-film thermoelectric cooler under the influence of the Thomson heating, the Joule heating, and the Fourier's heat conduction. A constant Thomson coefficient, instead of traditionally a constant Seebeck coefficient, is assumed. The influence of the Thomson effect on the cooling power, the achievable temperature difference and the optimum operating current density is then explored. It is found that the Joule's heat and the conduction heat flowing to the cold junction can be significantly reduced if thermoelectric materials with properly designed Thomson coefficients are employed. A modified thermal conductance and a modified electric resistance are resulted.

The second part of this paper details the analysis of the thermal stresses existing in the layered structure and induced by the temperature difference via a non-coupled thermal elastic theory. The results provide a preliminary knowledge to judge whether the thin-film structure is destroyed by the thermal stresses or not, especially by the shear stresses between adjacent layers.

Keywords: Thermoelectric cooler; Thomson effect; Thermal analysis; Thermal stress

1. Introduction

Thermoelectric coolers have advantages over the traditional heat pumps because they are compact and highly reliable, have no moving parts, and use no refrigerants. The poor cooling efficiency, which is fundamentally limited by the material properties, of thermoelectric devices, however, limits their applications. Basically, the cooling power arises from the Peltier effect and is degraded by the Fourier's conduction heat due to the existing temperature difference and by the Joule's heat due to the electric resistance. A material with a large Seebeck coefficient (α), a large electrical conductivity (σ), and a small thermal conductivity (k) is thus preferred. In fact, a conventional thermal analysis, taking the Fourier's conduction heat transfer, the Joule's heating, and sometimes the radiation and convection heat transfer between the thermoelectric element and the ambient gas into consideration [1–3], shows that thermoelectric materials are estimated by their ZT values (figure-of-merit), where T is the absolute temperature and $Z = \sigma\alpha^2/k$. The commonly known thermoelectric materials have ZT values between 0.6 and 1.0 at room temperature. It is believed that practical applications could be many more if materials with ZT values greater than 3 could be developed.

Various efforts [4–7] have been made to develop materials with higher ZT values. Recently, some exciting results have been reported at the material research society meetings for $ZT \geq 2$ in use of some low-dimensional materials such as quantum wells, quantum wires, quantum dots, and superlattice structures [8–15]. The increase in the ZT values is explained by the belief that reduced dimensionality changes the band structures (enhances the density of states near the Fermi energy), modifies the phonon dispersion relation, and increases the interface scattering of phonons. Consequently, the electric resistance and the lattice thermal conductivity [16–19] are both reduced, particularly the latter. In labs, thin-film/superlattices thermoelectric devices with very small dimensions have been fabricated using microelectronics technology and quantum wires are in fabricating.

A careful examination on the conventional thermal analysis finds that the temperature dependence of the Seebeck coefficient

* Corresponding author. Tel.: +886 2 3366 2696; fax: +886 2 2363 1755.
E-mail address: mjhuang@ntu.edu.tw (M.-J. Huang).

0924-4247/$ – see front matter © 2005 Elsevier B.V. All rights reserved.
doi:10.1016/j.sna.2005.10.006

is usually ignored and therefore the Thomson effect (charge carriers must absorb or release heat in order to overcome the non-homogeneity caused by the temperature gradients in the semiconductor) is not considered [20,21]. Nonetheless, the temperature dependence of the Seebeck coefficient is often observed in the labs [22–24] and the temperature gradients exist surely in a thermoelectric device. Hsu et al. [22] measured the thermoelectric properties of bulk $AgPb_{10}SbTe_{12}$. From their Fig. 2A, the Thomson coefficient is estimated to be about the same as the Seebeck coefficient (≈200 μV/K). The temperature dependence of bismuth films of different thicknesses was explored by Damodara and Soundararajan [23]. Their measurements also showed a Thomson coefficient on the order in magnitude of the Seebeck coefficient. The signs are the same near the room temperature but opposite at higher temperatures. Experimental data obtained by Rowe et al. [24] for intermediate valence compound $YbAl_3$ [24] shows similar results.

Not impossible is that the reversible Thomson heat changes the temperature profile in the thermoelectric element and modifies the associated thermal conductance and electric resistance, resulting in a better thermal performance [25,26]. This constitutes the motivation of the present study, to investigate the influence of the Thomson effect on the performance of a thin-film thermoelectric cooler. On the other hand, although a better thermal performance is targeted, the thermal stresses induced by the raised temperature difference may be harmful [27]. Above all, the induced shear stresses between adjacent thin-film layers may tear the layered structure. A one-dimensional thermal stress analysis therefore will also be performed.

This paper is arranged as follows. The thermal model adopted is described and the thermal performance in the presence of the Thomson effect is investigated in Section 2. The thermal stress analyses, including the normal stresses and the shear stresses, are performed through a non-couple elastic theory and presented in Section 3. Conclusions are given at last in Section 4.

2. Thermal analysis

2.1. Thermal model

Considered herein is a thin-film thermocouple similar to that analyzed by Völklein et al. in 1999 [3]. Fig. 1 shows the cross-section of the structure, including the supporting membrane and the p-type and n-type thermoelectric films that are separated by an insulating layer. As mentioned by Völklein et al. [3], because the thickness of the membrane, of the thermoelectric films, and of the insulating layer are very thin compared to the length L, the temperature variations in the thickness direction are expected to be negligible. Therefore, a one-dimensional thermal analysis is adopted. Moreover, in order to highlight the Thomson effect, the radiation and convection heat transfer between the thermocouple and the ambient gas is ignored in the present study. All the thermoelectric properties of the employed materials are assumed to be constant, except the Seebeck coefficient. The Seebeck coefficient (α) instead is assumed to have a logarithmic dependence on the temperature, that is

Fig. 1. The cross-section of the thin-film thermocouple under investigation.

$$\alpha = \alpha_0 = \beta \ln \frac{T}{T_0} \tag{1}$$

where α_0 is the Seebeck coefficient at some reference temperature T_0. In other words, it is the Thomson coefficient, β, that is assumed to be temperature-independent [20].

According to the non-equilibrium thermodynamics and following the analysis of Völklein et al. [3], one can write down the governing equation of the steady temperature distribution $T(x)$ in the thermocouple as follows:

$$0 = \frac{\mathrm{d}}{\mathrm{d}x}\left((kA)_\mathrm{t}\frac{\mathrm{d}T}{\mathrm{d}x}\right) + \frac{I^2}{(\sigma A)_\mathrm{pn}} - \beta_\mathrm{pn} I \frac{\mathrm{d}T}{\mathrm{d}x} \tag{2}$$

where I is the operating electric current, flowing from $x=0$ to $x=L$ in the p-type semiconductor and from $x=L$ to $x=0$ in the n-type semiconductor; $\beta_\mathrm{pn} = \beta_\mathrm{p} - \beta_\mathrm{n}$ and

$$(kA)_\mathrm{t} \equiv k_\mathrm{p}A_\mathrm{p} + k_\mathrm{i}A_\mathrm{i}k_\mathrm{n}A_\mathrm{n} + k_\mathrm{m}A_\mathrm{m} \tag{3}$$

$$\frac{1}{(\sigma A)_\mathrm{pn}} \equiv \frac{1}{\sigma_\mathrm{p}A_\mathrm{p}} + \frac{1}{\sigma_\mathrm{n}A_\mathrm{n}} \tag{4}$$

The subscripts m, p, n, and i represent the membrane, the p-type, the n-type, and the insulating layer, respectively. Finally, A is the cross-sectional area of each layer. Terms on the right-hand-side of Eq. (2) are the net axial Fourier's conduction heat transfer rate, the Joule's heat generation rate, and the Thomson heat generation rate, respectively.

With the boundary conditions $T(0) = T_\mathrm{c}$ (the cold-junction temperature) and $T(L) = T_\mathrm{h}$ (the hot-junction temperature), the solution of Eq. (2) is found to be

$$\frac{T(x) - T_\mathrm{c}}{T_\mathrm{h} - T_\mathrm{c}} = (1-\zeta)\frac{1 - \exp\left(\xi\frac{x}{L}\right)}{1 - \exp(\xi)} + \zeta\frac{x}{L} \tag{5}$$

where $\xi = \beta_\mathrm{pn}I/K_\mathrm{t}$ and $\zeta \equiv IR_\mathrm{t}/\beta_\mathrm{pn}(T_\mathrm{h} - T_\mathrm{c})$ are the ratio of the associated Thomson heat to the Fourier's conduction heat and the ratio of the Joule's heat to the Thomson heat. The "intrinsic" thermal conductance and electric resistance of the thermocouple (those in the absence of the Thomson effect) are designated as $K_\mathrm{t} \equiv (kA)_\mathrm{t}/L$ and $R_\mathrm{t} \equiv L/(\sigma A)_\mathrm{pn}$. When the Thomson effect is absent, Eq. (5) is reduced to

$$\frac{T(x) - T_\mathrm{c}}{T_\mathrm{h} - T_\mathrm{c}} = \frac{1}{2}\xi\zeta\left(\frac{x}{L} - \frac{x^2}{L^2}\right) + \frac{x}{L} \tag{6}$$

in which the ratio of the Joule's heat to the Fourier's conduction heat (=$\xi\zeta$) alone determines the temperature distribution. The influence of the Thomson heat on the temperature profiles is shown in Fig. 2, in which $\xi\zeta$ is fixed to be 2 such that the dimensionless temperature distribution, Eq. (6), has a maximum value of 1 at $x=L$. An increasing temperature gradient near $x=L$ and a decreasing one near $x=0$ with an increasing positive ξ are

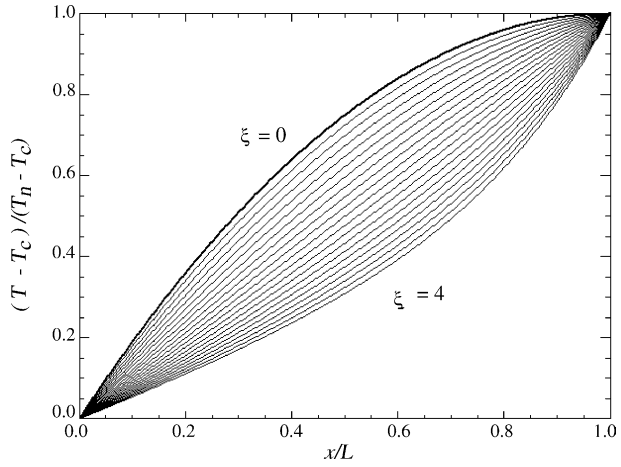

Fig. 2. The dimensionless temperature profiles within the thermoelectric element under several ratios of the Thomson heat to the Fourier's conduction heat (ξ) with $\xi\zeta = 2$ fixed.

observed. The latter implies an improved thermal performance of the thermoelectric cooler by the Thomson effect.

Based on the temperature distribution, Eq. (5), the Fourier's heat flow rate at the cold junction can be calculated and written as

$$(kA)_t \left.\frac{\partial T}{\partial x}\right|_{x=0} = \tilde{K}(T_h - T_c) + \tilde{R}I^2/2 \tag{7}$$

where $\tilde{K} \equiv \eta_K(\xi)K_t$ and $\tilde{R} \equiv \eta_R(\xi)R_t$ are the modified (effective) thermal conductance and the modified (effective) electric resistance. The modification factors are

$$\eta_K(\xi) = \frac{\xi}{e^{\xi} - 1} \tag{8}$$

$$\eta_R(\xi) = \frac{2}{\xi} - \frac{2}{e^{\xi} - 1} \tag{9}$$

and are shown in Fig. 3. It is interesting to see that both decrease with increasing positive ξ_{pn}. Finally, the allowable heat load

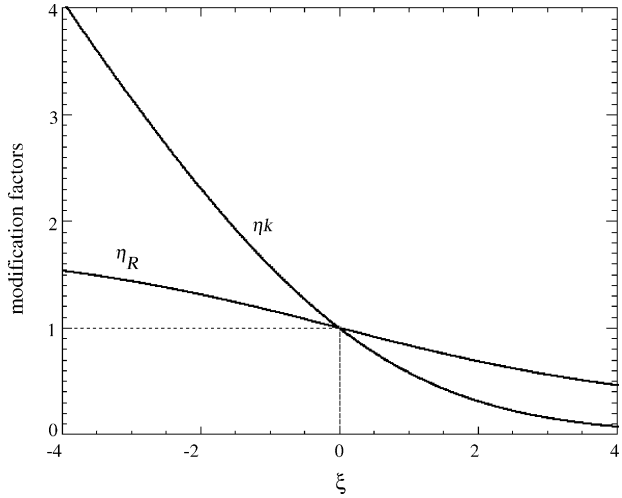

Fig. 3. The modification factors of the thermal conductance and the electric resistance due to the Thomson effect.

under a given temperature difference $\Delta T = T_h - T_c$ and an operating current I is computed as

$$N = \alpha_{pn} I T_c - \tilde{K}(T_h - T_c) - \tilde{R}I^2/2 \tag{10}$$

2.2. Thermal performance

The performance of a thermoelectric cooler is judged by its maximum achievable temperature difference ΔT_{max} or by its maximum allowable heat load N_{max}. The former is the maximum temperature difference that can be achieved under no external heat load as the operating current varies. From Eq. (10), it can be shown that the maximum achievable temperature difference ΔT_{max} and the corresponding optimum operating current $I_{opt.T}$. are determined by

$$Z_c T_c = \frac{\alpha_{pn}}{\beta_{pn}}(1 - e^{-\xi_{opt.T}}) \tag{11}$$

and

$$Z_c \Delta T_{max} = \frac{\alpha_{pn}^2}{\beta_{pn}^2}\{\xi_{opt.T} + \exp(-\xi_{opt.T}) - 1\} \tag{12}$$

where $\xi_{opt.T} \equiv \beta_{pn} I_{opt.T}/K_t$, $\alpha_{pn} = \alpha_p - \alpha_n$ and $Z_c \equiv \alpha_{pn}^2/K_t/R_t$ (evaluated at the cold-junction temperature T_c). For a comparison, the counterparts when the Thomson effect is absent are written below:

$$I_{opt.T} = \frac{\alpha_{pn} T_c}{R_t} \tag{13}$$

$$\Delta T_{max} = \frac{1}{2} Z_c T_c^2 \tag{14}$$

Fig. 4 shows one illustration. The material properties employed by Völklein et al. [3] are referred. They are: $\sigma_{p,n}^{-1} = 13.3\,\mu\Omega$ /m, $k_{p,n} = 1.28$ W/mK, $k_{i,m} = 2.0$ W/mK, and $\alpha_{pn} = 370\,\mu$V/K at $T_c = 250$ K. The thermocouple dimensions are chosen to be $A_{i+m} = 0.2\,\text{mm} \times 3\,\mu\text{m} \times 2$, $A_{p,n} = 0.2\,\text{mm} \times 10\,\mu\text{m}$, and $L = 0.3$ mm. As seen, the maximum achievable temperature difference is increased by a positive β_{pn}. It is about 42.8 K when $\beta_{pn} = 0$ and about 57.5 K when $\beta_{pn} = 400\,\mu$V/K. This is because

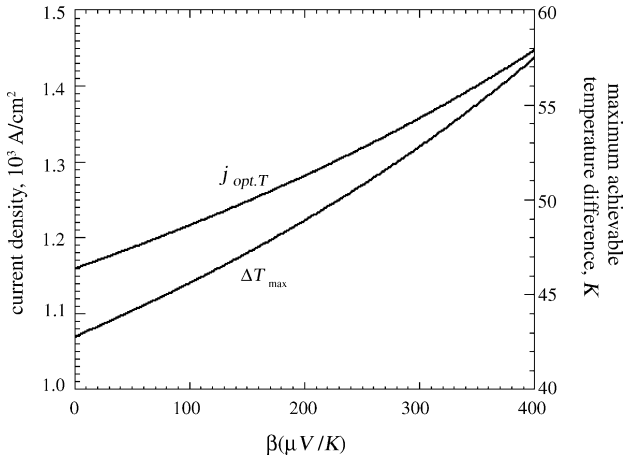

Fig. 4. The influence of Thomson effect on the maximum achievable temperature difference and the corresponding optimum operating current density.

the current absorbs heat not only at the cold-junction through the Peltier effect but also all the way along the thermoelectric element due to the Thomson effect. The amounts of Joule's heat and Fourier's conduction heat flowing to the cold junction are consequently decreased by factors of η_R and η_K, respectively.

The maximum allowable heat load, N_{max}, is defined as the maximum heat load under $\Delta T = 0$ as the operating current I varies. Substituting Eqs. (8) and (9) into Eq. (10), one finds that

$$Z_c T_c = \frac{\alpha_{pn}}{\beta_{pn}} \left(1 + \frac{\xi_{opt.N}^2 \exp \xi_{opt.N}}{(1 - \exp \xi_{opt.N})^2} + \frac{2\xi_{opt.N}}{1 - \exp \xi_{opt.N}} \right) \quad (15)$$

and

$$Z_c N_{max} = K_t \frac{\alpha_{pn}^2}{\beta_{pn}^2} \frac{\xi_{opt.N}^2}{(1 - \exp \xi_{opt.N})} \left(1 + \frac{\xi_{opt.N} \exp \xi_{opt.N}}{1 - \exp \xi_{opt.N}} \right) \quad (16)$$

where $\xi_{opt.N} = \beta_{pn} I_{opt.N}/K_t$ is the corresponding optimum dimensionless operating current. The counterparts as $\beta_{pn} = 0$ are

$$I_{opt.N} = \frac{a_{pn} T_c}{R_t} \quad (17)$$

and

$$N_{max} = \frac{1}{2} K_t Z_c T_c^2 \quad (18)$$

Note that the two optimum operating currents, computed from Eqs. (11) and (15), are in general different. Eqs. (13) and (17) however, are the same. Fig. 5 shows another illustration. The thermocouple used in Fig. 4 is employed again but the thermoelectric properties are evaluated at $T_c = T_h = 293$ K now and they are: $\alpha_{pn} = 460\ \mu V/K$, $\sigma_{p,n}^{-1} = 17\ \mu\Omega/m$, $k_{p,n} = 108$ W/mK, and $k_{i,m} = 2.2$ W/Mk. The maximum allowable heat load is found to be 17.8 mW as $\beta_{pn} = 0$ and is 19.4 mW when $\beta_{pn} = 400\ \mu V/K$. One may notice that the maximum allowable heat load is not improved as much as the maximum achievable temperature difference is. This is because the temperature gradient is now positive near $x = 0$ and negative near $x = L$ (the peak temperature occurs somewhere in the middle of the thermocouple). The Thomson effect works on shifting the peak temperature toward the hot junction and reducing the peak value as seen from Fig. 6, in which the temperature profiles, Eqs. (5) and (6), are re-plotted with $\Delta T = 0$. As a result, the current absorbs heat somewhere but releases heat somewhere else along the thermocouple. The net improvement is thus not much.

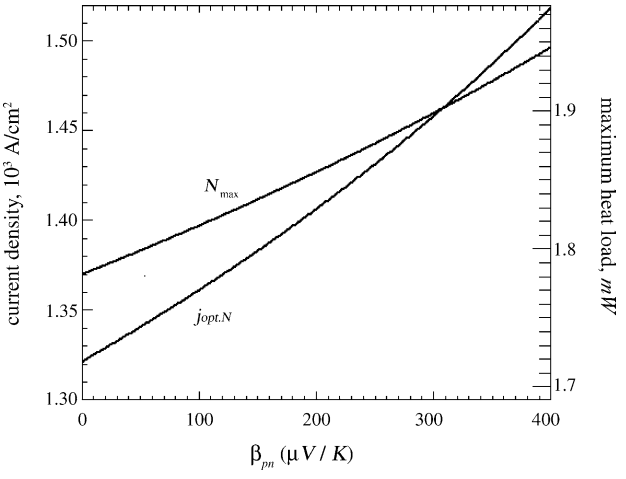

Fig. 5. The influence of Thomson effect on the maximum allowable heat load and the corresponding optimum operating current density.

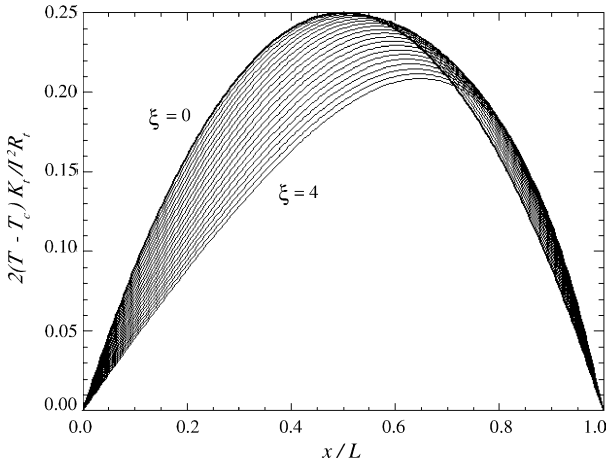

Fig. 6. The influence of Thomson effect on the temperature profiles when the temperature difference across the thermoelectric element is zero.

3. Thermal stress analysis

3.1. Thermal stress model

Like the thermal analysis performed in the previous section, it is also assumed that the thermal displacement occurs mainly in the x-direction and its variation across the thickness direction is much smaller than that in the x-direction; that is, $u \gg w$ and $\partial/\partial x \gg \partial z$. The free stress temperature (T_{fs}) is set at 293 K and non-elastic effects such as plasticity and creep are not taken into consideration. The thermoelectric element is next assumed to be clamped at both junctions and free at the top and bottom surfaces. Consequently, a force balance over a control volume as shown in Fig. 7 results in

$$\frac{dA_p \sigma_{xx,p}}{dx} + \frac{dA_i \sigma_{xx,i}}{dx} + \frac{dA_n \sigma_{xx,n}}{dx} + \frac{dA_m \sigma_{xx,m}}{dx} = 0 \quad (19)$$

where σ_{xx} is the normal stress and is related to the x-displacement $u(x)$ by

$$\sigma_{xx} = E \left(\frac{du}{dx} - \gamma (T - T_{fs}) \right) \quad (20)$$

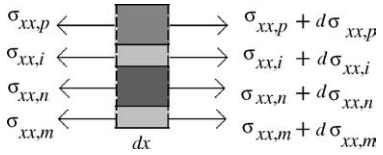

Fig. 7. The control volume for the thermal stress analysis.

with E being the Young's modulus and γ being the thermal expansion coefficient. Substituting Eq. (20) into Eq. (19), one obtains

$$\frac{d^2u}{dx^2} = \gamma_0 \frac{dT}{dx} \tag{21}$$

where

$$\gamma_0 = \frac{A_p E_p \gamma_p + A_i E_i \gamma_i + A_n E_n \gamma_n + A_m E_m \gamma_m}{A_p E_p + A_i E_i + A_n E_n + A_m E_m} \tag{22}$$

is the weighted average of the thermal expansion coefficients. The solution of Eq. (21) with clamped junctions is easily found to be

$$\frac{u(x)}{L\gamma_0 \Delta T} = \frac{\zeta}{2}\frac{x}{L}\left(\frac{x}{L} - 1\right) + \frac{1-\zeta}{\xi}\left(\frac{1-\exp \xi \frac{x}{L}}{1-\exp \xi} - \frac{x}{L}\right) \tag{23}$$

By substituting Eq. (23) into Eq. (20), one obtains the normal-stress distribution as follows:

$$\sigma_{xx} = E\{\gamma_0(T - T_0) - \gamma(T - T_{fs})\} \tag{24}$$

where the current-dependent temperature T_0 is a linear combination of the junction temperatures,

$$T_0 = \phi T_h + (1 - \phi)T_c \tag{25}$$

The fraction ϕ is

$$\phi = \frac{1-\zeta}{1-\exp\xi} + \frac{1-\zeta}{\xi} + \frac{\zeta}{2} \tag{26}$$

when $\beta \neq 0$ and

$$\phi = \frac{1}{2} + \frac{1}{12}\xi\zeta \tag{27}$$

when $\beta = 0$. An examination on Eqs. (24) and (20) shows that the temperature T_0 appears at the location where the maximum displacement occurs. The temperature T_0 may be viewed as a "free-structure-stress" temperature. Actually, Eq. (24) implies that the thermal stress within each layer can be divided into two parts. The first part is caused purely by the local temperature change as if there were no adjacent layers. The second part on the other hand is induced by the mutual influence between layers due to the layered structure. It vanishes if the temperature is equal to T_0.

Fig. 8 shows the influence of the Thomson effect on the thermal displacement. It is observed that the location where the maximum displacement or T_0 appears shifts toward the hot junction as the Thomson effect increases. The dependence of the fraction ϕ on the parameter ξ with several fixed values of $\xi\zeta$ is shown in Fig. 9. Basically, the fraction ϕ, or $(T_0 - T_c)/(T_h - T_c)$, decreases with increasing Thomson effect. The above two observations together imply a reduced temperature gradient at the cold junction and consequently an improved thermal performance.

At last, presented in Fig. 10 are the normal-stress distributions along the thermoelectric element operated at the optimum current shown in Fig. 5. The thermo-mechanical properties of semiconductor $Si_{0.5}Ge_{0.5}$ are employed for the p-type as well as the n-type thin-film ($E = 160$ Gpa and $\gamma = 4.2 \times 10^{-6}$/K) and

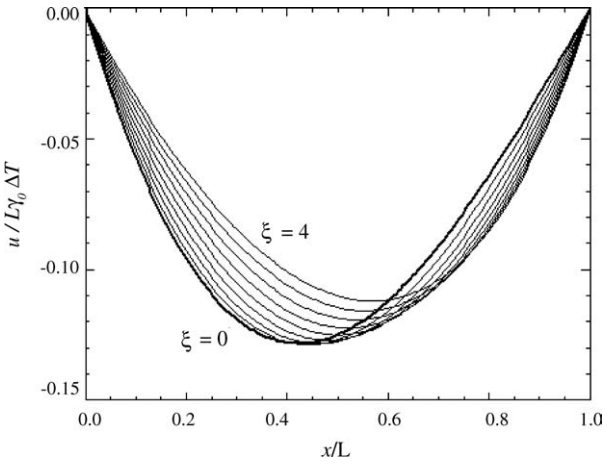

Fig. 8. The dimensionless displacement along the thermoelectric element under several ratios of the Thomson heat to the Fourier's conduction heat (ξ) with $\xi\zeta = 2$ fixed.

those of SiO_2 are used for the membrane and the insulating thin-film ($E = 160$ Gpa and $\gamma = 5 \times 10^{-7}$/K). As seen, with increasing Thomson effect, the absolute normal stresses increase. All the calculated normal stresses are under the yielding stresses of the materials in use nonetheless.

3.2. Shear stresses

The shear stresses between adjacent layers can be found now by taking a force balance for each layer. The result is

$$\tau_{zx}(x, z = h) = -\frac{dh\sigma_{xx}}{dx} + \tau_{zx}(x, z = 0) \tag{28}$$

where h is the thickness of the layer of interest. Because the top and the bottom surfaces of the thermoelectric element are assumed to be free, the shear stresses are found to be

$$\tau_{m,n} = -E_m h_m(\gamma_0 - \gamma_m)\frac{dT}{dx} \tag{29}$$

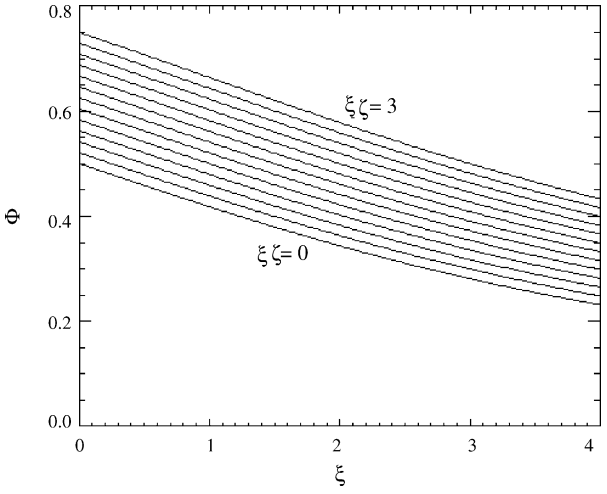

Fig. 9. The function ϕ against the Thomson-effect parameter ξ when the value of $\xi\zeta$ is fixed (the increment is $\Delta\xi\zeta = 0.25$).

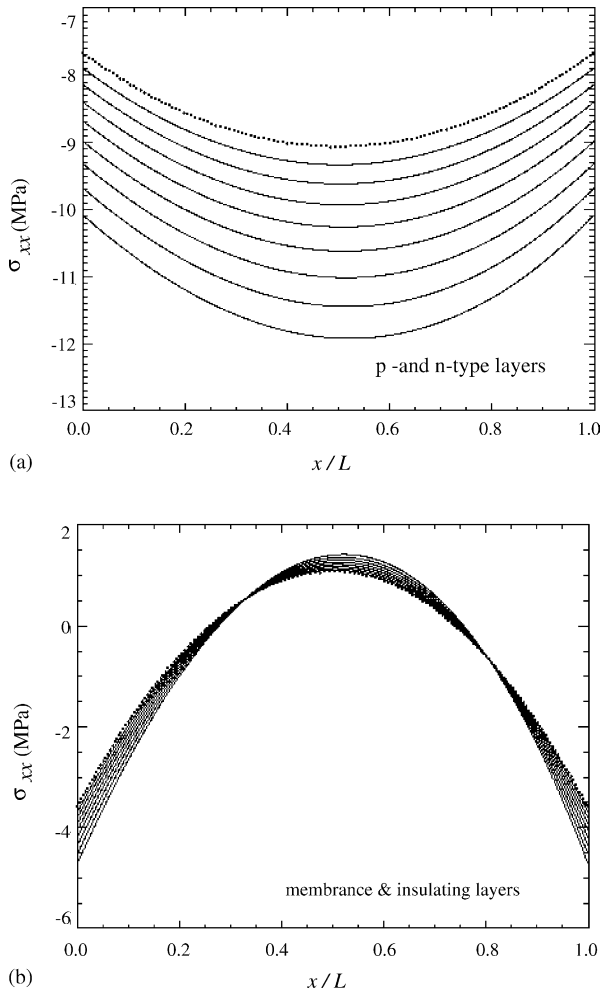

Fig. 10. The normal-stress distributions of the thermoelectric element operated at the optimum currents shown in Fig. 5, where $\Delta\beta_{pn} = 50\,\mu V/K$ and $\beta_{pn,max} = 400\,\mu V/K$. The dotted curve is the one corresponding to $\beta_{pn} = 0$.

$$\tau_{n,i} = -[E_n h_n(\gamma_0 - \gamma_n) + E_m h_m(\gamma_0 - \gamma_m)]\frac{dT}{dx} \tag{30}$$

and

$$\tau_{i,p} = -[E_i h_i(\gamma_0 - \gamma_i) + E_n h_n(\gamma_0 - \gamma_n) + E_m h_m(\gamma_0 - \gamma_m)]\frac{dT}{dx} \tag{31}$$

Alternatively, the shear stress between the insulating layer and the p-type layer can be written as

$$\tau_{i,p} = E_p h_p(\gamma_0 - \gamma_p)\frac{dT}{dx} \tag{32}$$

due to Eq. (19). Eqs. (29)–(32) indicate that the magnitude of the shear stress is proportional to the temperature gradient. In addition, the larger the heterogeneity in the thermal expansion coefficients of materials, the larger the shear stress is resulted. From Fig. 2, the location where the maximum temperature gradient appears moves gradually from the cold junction to the hot junction as the Thomson effect increases. Fig. 11 shows the shear stress distributions corresponding to the normal-stress distributions in Fig. 10. Because of the materials used, the shear stress

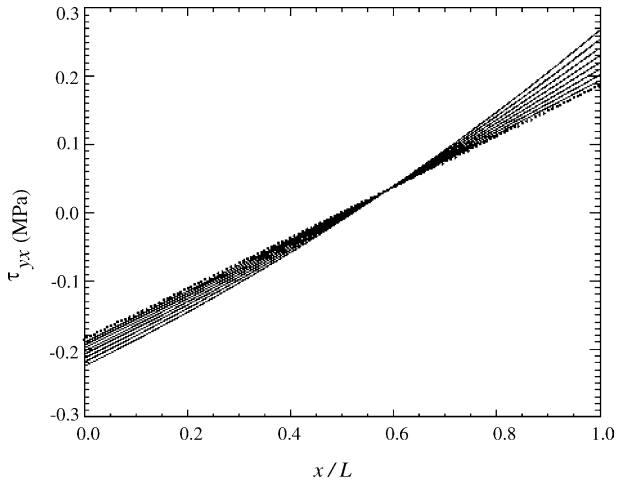

Fig. 11. The shear stress distributions between the insulating layer and the p-type semiconductor as the thermoelectric cooler is operated at the optimum currents shown in Fig. 5, where $\Delta\beta_{pn} = 50\,\mu V/K$ and $\beta_{pn,max} = 400\,\mu V/K$. The dotted curve is the one corresponding to $\beta_{pn} = 0$.

distribution between the p-type layer and the insulating layer is the same as that between the membrane layer and the n-type semiconductor. Furthermore, the shear stress between the n-type semiconductor and the insulating layer vanishes. Therefore, only one distribution for each Thomson coefficient is plotted in Fig. 11. These calculations show that the magnitudes of the shear stresses near the hot junction increase more rapidly than those near the cold junction. It is again because the current absorbs heat near the cold junction and releases heat near the hot junction by the Thomson effect, causing larger temperature gradients (as observed in Fig. 6) and thus larger shear stresses near the hot junction.

4. Conclusion

The thermal performance of a thin-film thermoelectric cooler under the influence of the Thomson heating, the Joule heating, and the Fourier's heat conduction is investigated. For those cases that the Thomson effect is important, two dimensionless influence parameters—the ratio of the Thomson heat to the conduction heat and the ratio of Joule's heat to the Thomson heat, determine the thermal performance. The conduction heat and the Joule's heat flowing to the cold junction can be significantly reduced, providing that the Thomson coefficient of the p-type layer is greater than that of the n-type. A larger maximum temperature difference can be achieved and a larger maximum heat load can be allowed consequently.

The normal-stress distributions within the thermoelectric element as well as the shear stress distributions between adjacent layers are also analyzed by a non-coupled elastic theory. A "free-structure-stress" temperature for the whole thin-film thermocouple is defined. It characterizes the mutual influence between layers. As the thermal performance is improved by the Thomson effect, the induced thermal stresses are increased as well. They cannot be greater than the yielding stresses of the materials in use for safety. Finally, it is found that the shear stress is proportional to the temperature gradient and the larger the heterogeneity in

the thermal expansion coefficients of materials, the larger the shear stress is resulted.

Acknowledgements

The support of this work by the National Science Council, Taiwan, ROC under contract NSC 92-2212-E-002-047 and ITRI under the contract 3000017521 are gratefulfly acknowledged.

References

[1] D.M. Rowe, CRC Handbook of Thermoelectrics, CRC Press LLC, 1995.
[2] C. LaBounty, A. Shakouri, J.E. Bowers, Design and characterization of thin film microcoolers, J. Appl. Phys. 89 (2001) 4059–4064.
[3] F. Völklein, Gao Min, D.M. Rowe, Modelling of a mircoelectromechanical thermoelectric cooler, Sens. Actuators 75 (1999) 95–101.
[4] G. Mahan, B. Sales, J. Sharp, Thermoelectric materials: new approaches to an old problem, Phys. Today 50 (3) (1997) 42.
[5] J.P. Fleurial, New Thermoelectric Materials and Devices: New Challenges, UCLA, 1997.
[6] R.G. Mahtur, R.M. Mehra, Thermoelectric power in porous silicon, J. Appl. Phys. 83 (1998) 5855–5857.
[7] D.G. Cahill, K. Goodson, A. Majumdar, Thermometry and thermal transport in micro/nanoscale solid-state devices and structures, J. Heat Transfer 124 (2002) 223–241.
[8] L.D. Hicks, M.S. Dresselhaus, Effect of quantum-well structures on the thermoelectric figure of merit, Phys. Rev. B 47 (1993) 12727–12731.
[9] L.D. Hicks, M.S. Dresselhaus, Thermoelectric figure of merit of a one-dimensional conductor, Phys. Rev. B 47 (1993) 631–634.
[10] B.C. Sales, Smaller is cooler, Science 295 (2002) 1248–1249.
[11] R. Venkatasubramanian, E. Silvola, T. Colpitts, B. O'Quinn, Thin-film thermoelectric devices with high room-temperature figures of merit, Nature 413 (2001) 597–602.
[12] D.J. Yao, In-plane MEMS thermoelectric micorcooler, Ph.D. Dissertation, UCLA, 2001.
[13] R. Livi, S. Lepri, Heat in one dimension, Nature 421 (2003) 327.
[14] G. Chen, A. Shakouri, Heat transfer in nanostructures for solid-state energy conversion, J. Heat Transfer 124 (2002) 242–252.
[15] M.S. Dresselhaus, Y.M. Lin, S.B. Cronin, O. Rabin, M.R. Black, G. Dresselhaus, T. Koga, Quantum wells and quantum wires for potential thermoelectric applications, Semicond. Semimetals 71 (2001) 1–121.
[16] G. Chen, Size and interface effects on thermal conductivity of superlattices and periodic thin-film structures, J. Heat Transfer 119 (1997) 220–229.
[17] G. Chen, Thermal conductivity and ballistic-phonon transport in the cross-plane direction of superlattices, Phys. Rev. B 57 (1998) 958–973.
[18] D.G. Cahill, W.K. Ford, K.E. Goodson, G.D. Mahan, A. Majumdar, H.J. Maris, R. Merlin, S.R. Phillpot, Nanoscale thermal transport, J. Appl. Phys. 93 (2003) 793–818.
[19] J. Zhou, A. Balandin, Phonon heat conduction in a semiconductor nanowire, J. Appl. Phys. 89 (2001) 2932–2938.
[20] S. Wisniewski, B. Staniszewski, R. Szymanik, Thermodynamics of nonequilibrium processes, PWN-Polish Scientific Publishers, 1976.
[21] S.L. Soo, Direct Energy Conversion, Prentice-Hall Inc, 1968.
[22] K.F. Hsu, S. Loo, F. Guo, W. Chen, J.S. Dyck, C. Uher, T. Hogan, E.K. Polychroniadis, M.G. Kanatzidis, Cubic $AgPb_mSbTe_{2+m}$: bulk thermoelectric materials with high figure of merit, Science 303 (2004) 818–821.
[23] V. Damodara Das, N. Soundararajan, Size and temperature effects on the Seebeck coefficient of thin bismuth films, Phys. Rev. B 35 (1987) 5990–5996.
[24] D.M. Rowe, V.L. Kuznetsov, L.A. Kuznetsova, G. Min, Electric and thermal transport properties of intermediate-valence $YbAl_3$, J. Phys. D 35 (2002) 2183–2186.
[25] J. Chen, Z. Yan, L. Wu, The influence of Thomson effect on the maximum power output and maximum efficiency of a thermoelectric generator, J. Appl. Phys. 79 (1996) 8823–8828.
[26] M.J. Huang, R.H. Yen, A.B. Wang, The influence of the Thomson effect on the performance of a thermoelectric cooler, Int. J. Heat Mass Transfer 48 (2005) 413–418.
[27] Y. Hori, D. Kusano, T. Ito, K. Izumi, Analysis on thermo-mechanical stress of thermoelectric module, in: Proceedings of the 18th International Conference on Thermoelectrics, 1999, pp. 328–331.

Biographies

Mei-Jiau Huang has Ph.D. in Mechanical Engineering from California Institute of Technology, CA, USA. Huang is Associate Professor, Department of Mechanical Engineering, National Taiwan University, Taipei, Taiwan. Huang's areas of interests include thermoelectrics, computational fluid dynamics, and vortex dynamics.

Po-Kuei Chou has M.S. degree in Mechanical Engineering from National Taiwan University, Taipei, Taiwan. Chou is an Engineer, Coretronic Corporation. Chou's areas of interests include thermoelectrics and optics.

Ming-Chyuan Lin has Ph.D. in Mechanical Engineering from National Tsing Hua University, Shinchu, Taiwan. Lin is Research Associate, National Synchrotron Radiation Research Center, Shinchu, Taiwan. Lin's areas of interests include cryogenic engineering, superconducting cavity, and solid mechanics.